Electronic Supplementary Material (ESI) for Journal of Materials Chemistry A.

Supplementary Information

Hierarchical Flower-like Co_2TiO_4 Nanosheets with Unique Structural and Compositional Advantages to Boost Peroxymonosulfate Activation for Degradation of Organic Pollutants

Haitao Li, Hao Wang, Qiang Gao*, Bo Han, Kaisheng Xia, Chenggang Zhou*

Faculty of Material Science and Chemistry, China University of Geosciences, Wuhan 430074, PR China

*Corresponding authors:

Tel./Fax: +86 027 6788 3731;

E-mail addresses: gaoqiang@cug.edu.cn (Q. Gao);
cgzhou@cug.edu.cn (C.G. Zhou).

Table S1 The catalytic performances of Co_2TiO_4 and previously reported heterogeneous cobalt-based catalysts for degradation OFX in the presence of PMS.

Catalyst	**Target pollutant**	**Pollutant concentration**	**Degradation efficiency**	***k*** **(min^{-1})**	**Ref.**
Co_3O_4 NP	OFX	18 mg L^{-1}	~100% within 60 min	0.06	[1]
BC-Co_3O_4	OFX	18 mg L^{-1}	~100% within 10 min	0.46	[1]
Mesoporous bouquet-like Co_3O_4	OFX	18 mg L^{-1}	~100% within 60 min	0.0054	[2]
Co-Fe-TiO_2	OFX	30 mg L^{-1}	~100% within 240 min	0.0278	[3]
$Co(OH)_2$/rGO	OFX	25 mg L^{-1}	~95% within 30 min	—	[4]
Co-Fe PBAs	OFX	20 mg L^{-1}	~80% within 30 min	—	[5]
$CoFe_2O_4$	OFX	20 mg L^{-1}	~70% within 30 min	—	[5]
Co_2TiO_4	OFX	25 mg L^{-1}	~100% within 30 min	1.394	This work

EXPERIMENTAL SECTION

Chemicals and Reagents

The chemicals, tert-butyl alcohol (TBA, ≥99%), methanol (≥99.9%), 5,5-dimethyl-pyrroline-oxide (DMPO, ≥97%), ofloxacin (OFX), norfloxacin (NFX), methyl orange (MO), rhodamine B (RhB), cobalt chloride hexahydrate ($CoCl_2{\cdot}6H_2O$), glycerol (Gly), ethylenediamine (EDA), NaCl, $NaNO_3$, Na_2SO_4, Na_2HPO_4, and $NaHCO_3$ were purchased from Sinopharm Chemical Reagent Co., Ltd. (Shanghai, China). Besides, commercial Co_3O_4 nanoparticles (99%), peroxymonosulfate (PMS, ≥47% $KHSO_5$ basis) were obtained from Aladdin Company, China. Titanium isopropoxide (TTIP, 98%), were provided by J&K Scientific Ltd. (Beijing, China). All these reagents were used as received without further purification or modification. Deionized water was used throughout our experiments.

Synthesis of hierarchical Co_2TiO_4 microspheres

In brief, 297.9 mg of $CoCl_2{\cdot}6H_2O$ were dissolved into 8 mL of EDA to obtain a clear solution (solution I). At the same time, 0.39 mL of TTIP was added to a mixed solution containing water (20 mL) and Gly (32 mL), and stirred vigorously until the solution became clear and transparent (solution II). Then, solution I and II were quickly mixed and transferred to a Teflon-lined stainless-steel autoclave (100 mL) which included 16 mL of NaOH solution. The sealed autoclave was heated at 200 ^{o}C in an oven for 24 h. Finally, the solid powders (Co_2TiO_4) were collected by centrifugation, washed fully with water and ethanol, and dried at 60 °C in a vacuum oven overnight.

Characterization of Samples

Micro-morphologies of the Co_2TiO_4 and other relevant samples were observed using the scanning electron microscopy (SEM, SU8010, Hitachi, Japan) and transmission electron microscopy (TEM, Philips CM12). X-ray diffraction (XRD) patterns were collected from a Simens XRD instrument (D8-FOCUS, Bruker, Germany) with Cu Kα radiation ($\lambda = 0.154060$ nm). Nitrogen adsorption/desorption analyses were performed on a Micromeritics ASAP2020 surface area analyzer at 77 K. The cyclic voltammetry (CV) analysis was carried out on an electrochemical workstation (Shanghai Chen Hua CHI660D) with Pt sheet as the electrode and Hg/HgO as the reference electrode, respectively, at a scan rate of 5 mV s^{-1}. The electrolyte solution was KOH aqueous solution (6 M) and the test voltage ranged from −0.1 to 0.4 V at 25 °C. X-ray photoelectron spectroscopy (XPS) measurements were performed using a VG Scientific ESCALAB Mark II spectrometer. The intermediates produced in the degradation processes were determined by liquid chromatograph combined with mass spectrometry (LC-MS, Q Exactive Hybrid Quadrupole-Orbitrap, Thermo Scientific, Bremen, Germany) in ESI positive mode. The analysis of F^- ions was conducted on a Dionex model ICS 2000 ion chromatograph (IC) equipped with an Ion Pac AS11-HC analytical column (4 × 250 mm). Electron paramagnetic resonance spectroscopy (EPR, Bruker A300) was used to examine the generation of reactive species. The amount of cobalt leaching was determined by the ICP–MS (Elan DRC-e).

Temperature-programmed conditions

Temperature-programmed reduction of hydrogen (H_2-TPR) measurement was conducted with an AutoChem II 2920 instrument (Micromeritics). 50 mg as-prepared samples were heated to 300 ^{o}C (10 ^{o}C min^{-1}) under a N_2 flow (30 mL min^{-1}), and kept at that temperature for 0.5 h. After cooling down to room temperature, a mixture of H_2/N_2 (10 vol.% 30 mL min^{-1}) was introduced. Subsequently, the temperature was raised to 700 ^{o}C (10 ^{o}C min^{-1}). The amount of hydrogen consumed was monitored with a thermal conductor detector.

Computational Methods

All the calculations were performed using the periodic density functional theory (DFT) package of Vienna Ab-initio Simulation Package (VASP) codes.[6] Spin-polarized calculations were employed using the generalized gradient approximation (GGA) with the Perdew-Burke-Ernzerhof (PBE) + U to describe the exchange-correlation energy and electron interactions.[7,8] The Brillouin zone integration was sampled with a 2×2×1 Monkhorst-Pack k-point mesh. The convergence of the total energy was set to 10^{-3} eV for structure optimization.[9] Bader charge analysis was carried out to obtain the charge distribution of the system. The adsorption energy was evaluated by the following equation.

$$\Delta \boldsymbol{E}_{\mathrm{ads}} = \boldsymbol{E}_{\mathrm{PMS\text{-}S}} - \boldsymbol{E}_{\mathrm{PMS}} - \boldsymbol{E}_{\mathrm{S}} \qquad (1)$$

where the $\boldsymbol{E}_{\mathrm{PMS\text{-}S}}$, $\boldsymbol{E}_{\mathrm{PMS}}$ and $\boldsymbol{E}_{\mathrm{S}}$ represent the total energy of PMS adsorbed on substrate (Co_2TiO_4 or Co_3O_4), PMS molecule and the substrate (Co_2TiO_4 or Co_3O_4), respectively. According to this equation, a negative ΔE_{ads} value indicates that the adsorption process is energetically favorable.

Evaluating Catalytic Performance of Co_2TiO_4 in PMS activation

Typically, the catalytic degradation tests were conducted in a 20 mL vial at temperatures of 25 °C. In each run, 5 mg of Co_2TiO_4 powders were suspended in 10 mL of aqueous solution (pH=7), containing a target pollutant in a given concentration (i.e., [OFX] = 25 mg L^{-1}, [NFX] = 25 mg L^{-1}, [MO] = 50 mg L^{-1}, [RhB] = 50 mg L^{-1}). Subsequently, PMS with concentration of 1 mM was added to trigger the pollutant degradation. At specified time interval, 0.5 mL of reaction solution were withdrawn, filtered by a syringe, and quenched with excess MeOH (1.5 mL). The concentrations of MO and RhB were determined at the maximum absorption peaks of 462 and 554 nm, respectively, on a UV–Vis spectrophotometer (Shimadzu, UV-1850). The concentrations of other organic pollutants were analyzed using a HPLC with a C18 column (Wondasil, 250 × 4.6 mm, 5 μm).

Analysis of intermediates and degradation pathway in OFX decomposition

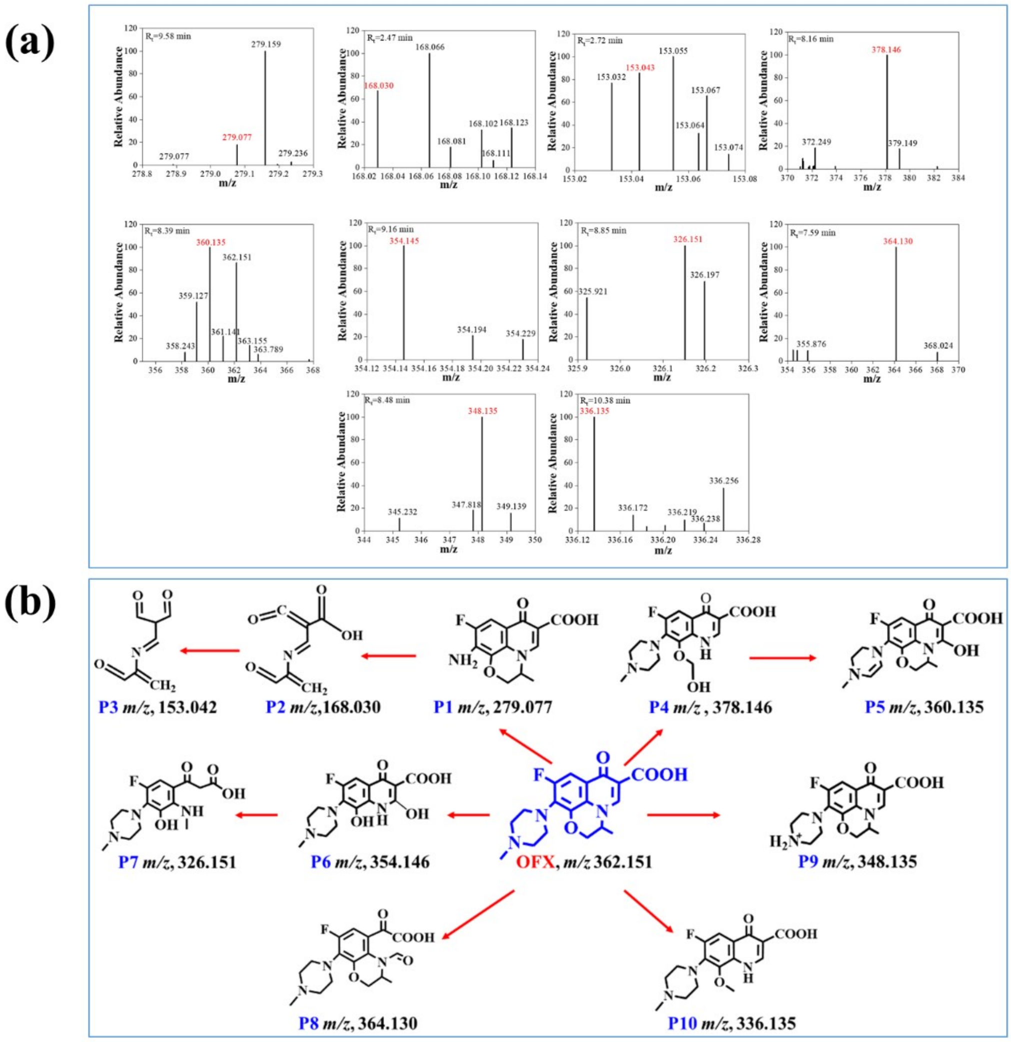

Fig. S1 Mass spectra of OFX and intermediate products (a), possible degradation pathway of OFX in Co_2TiO_4/PMS system (b).

As OFX can be rapidly degraded by Co_2TiO_4-activated PMS, it is of interest to investigate the corresponding degradation pathway of OFX. Fig. S1a shows the identification results on OFX and its intermediate products during catalytic degradation determined by LC/MS. Clearly, the characteristic peak of MNZ (*m*/*z* = 362.151) disappears after 30 min, and several new LC/MS signals are detected, indicating the OFX compounds are completely broken into intermediates and further mineralized. Based on these results, a plausible degradation pathway is proposed and shown in Fig. S1b. When OFX is present in Co_2TiO_4/PMS system, a part of OFX molecules might undergo oxidation of the N-piperazine ring to form an intermediate product P1 (*m*/*z* = 279.077).[10] The intermediate product P2 (*m*/*z* = 168.030) is produced by subsequent bond cleavage of P1.[11] Due to further oxidation of P2, the intermediate product P3 (*m*/*z* = 153.042) can be obtained. Upon insertion of a hydroxyl group into the OFX molecular structure, the intermediate product P4 with *m*/*z* of 378.146 appears, possessing one more O atom and one more H atom as compared to the parent OFX molecule.[12,13] Subsequently, loss of two hydrogens and primary alcohol leads to the formation of P5 (*m*/*z* = 360.135).[14] The intermediate product P6 (*m*/*z* = 354.146), with heterocyclic ring-C, should result from the transformation of OFX via a ring opening reaction with loss of three carbon atoms from the morpholine ring. Afterward, heterocyclic ring is destroyed, resulting in the production of smaller molecular weight intermediate product P7 (*m*/*z* = 326.151).[15] Besides, similar destruction reactions of the heterocyclic ring of OFX occur to yield intermediate product P8 (*m*/*z* = 364.130). In addition, the intermediate products of P9 (*m*/*z* = 348.135) and P10 (*m*/*z* = 336.135) are generated by successive removal of alkyl groups from OFX. Finally, these simple intermediate molecules will be further decomposed and mineralized.

Evaluation of mineralization degree of OFX degradation

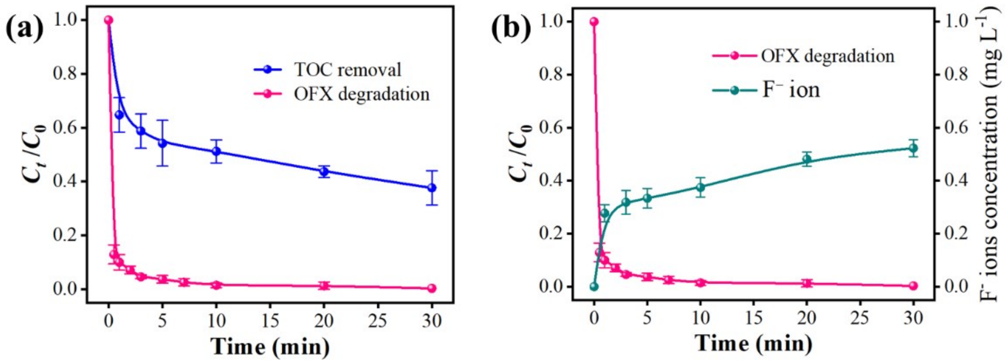

Fig. S2. TOC removal (a) and the generation of F^- ions (b) in OFX degradation process. (Experimental conditions: V=10 mL, C_{OFX}=25 mg L^{-1}, pH=7, $C_{catalyst}$=0.5 g L^{-1}, C_{PMS}=1 mM, t=25 °C)

The degree of mineralization was evaluated via TOC analyzer and ion chromatograph. As seen in Fig. S2, about 60% of TOC content was removed within 30 min meanwhile about 40% of F atoms in OFX molecules are converted into F^- ions, indicating the original structures of OFX molecules should be severely decomposed.

Optimized structures of DFT models

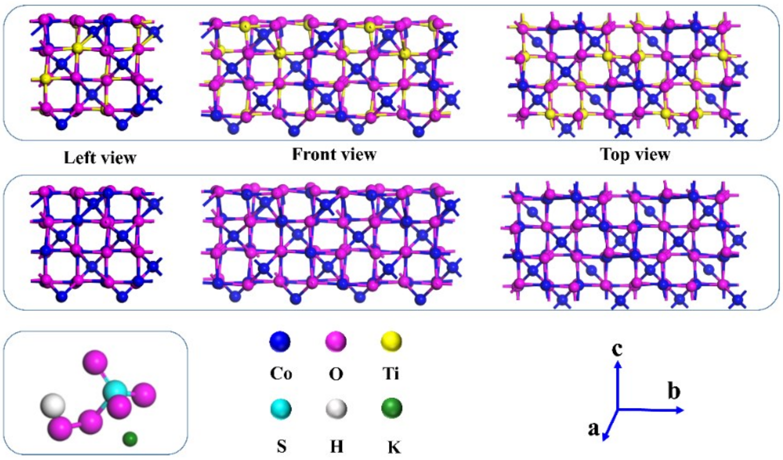

Fig. S3. The left, front, and top views of the optimized structures of (100) surfaces of cubic spinel Co_2TiO_4 (a) and Co_3O_4 (b), and free PMS molecule (c).

The commonly exposed (100) surfaces of spinel Co_2TiO_4 and Co_3O_4 are selected to establish structural models. Three views of the optimized structures of (100) surfaces of cubic spinel Co_2TiO_4 and Co_3O_4, and free PMS molecule are depicted in Fig. S3.

DFT models of PMS molecule adsorption process

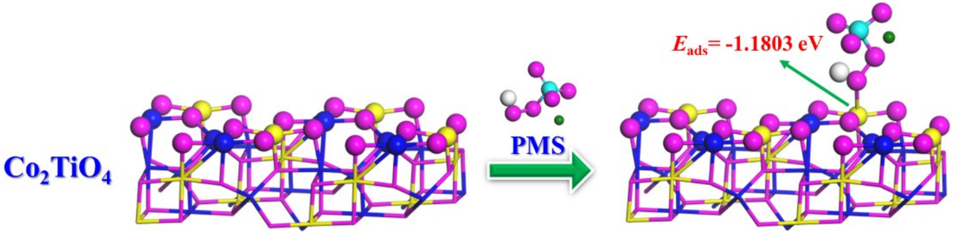

Fig. S4. DFT models of Co_2TiO_4 without and with a PMS molecule adsorption on the Ti site.

Cobalt leaching analysis and corresponding catalytic activity test.

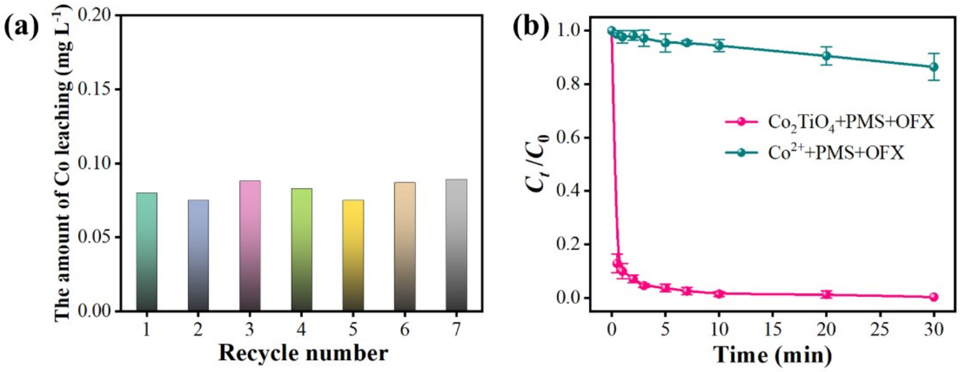

Fig. S5. Cobalt leaching amounts after each cycling experiment (a), degradation efficiency of OFX in different systems (b). (Experimental conditions: V=10 mL, C_{OFX}=25 mg L^{-1}, pH=7, C_{catalyst}=0.5 g L^{-1} $C_{\mathrm{Co}^{2+}}$=0.080 mg L^{-1}, C_{PMS}=1 mM, t=25 $^{\mathrm{o}}$C)

Characterization of used Co_2TiO_4 microspheres

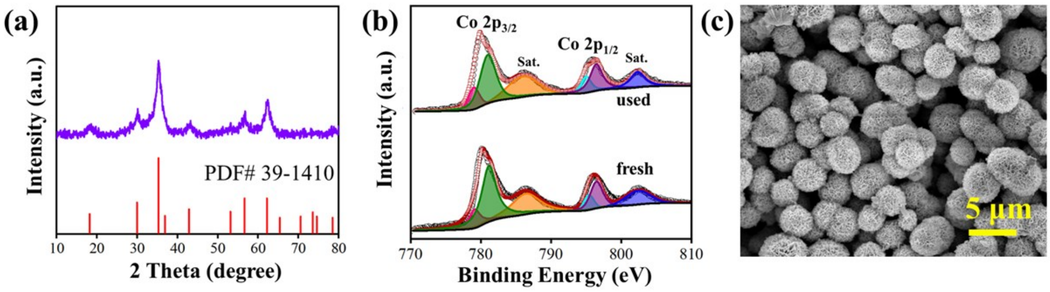

Fig. S6. XRD pattern (a), Co 2p spectra (b), and SEM image (c) of Co_2TiO_4 after used.

As show in Fig. S6a, the used catalyst still exhibits XRD diffraction peaks of spinel Co_2TiO_4 phase, where the peak positions and intensities are nearly invariant as compared to those of the fresh catalyst. Moreover, no obvious changes are detected between the Co 2p spectra of fresh Co_2TiO_4 and that after used (Fig. S6b). The nanosheets-assembled 3D flower-like architecture of the reused catalyst is well preserved during reuse without occurrence of any structural damage (Fig. S5c). Overall, these investigations indicate that the developed Co_2TiO_4 catalyst has great potential for scale-up application in long-term wastewater treatment.

OFX degradation in actual water matrix

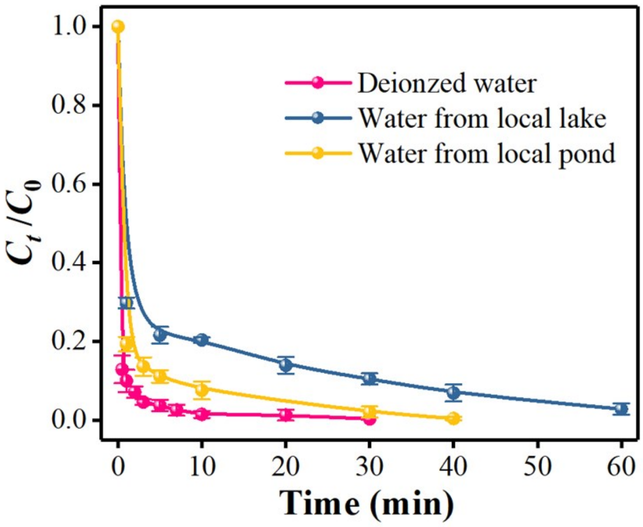

Fig. S7. OFX degradation in real water matrix. (Experimental conditions: V=10 mL, C_{OFX}=25 mg L^{-1}, pH=7, C_{catalyst}=0.5 g L^{-1}, C_{PMS}=1 mM, t=25 °C)

Zeta potential analysis and solution pH evaluation

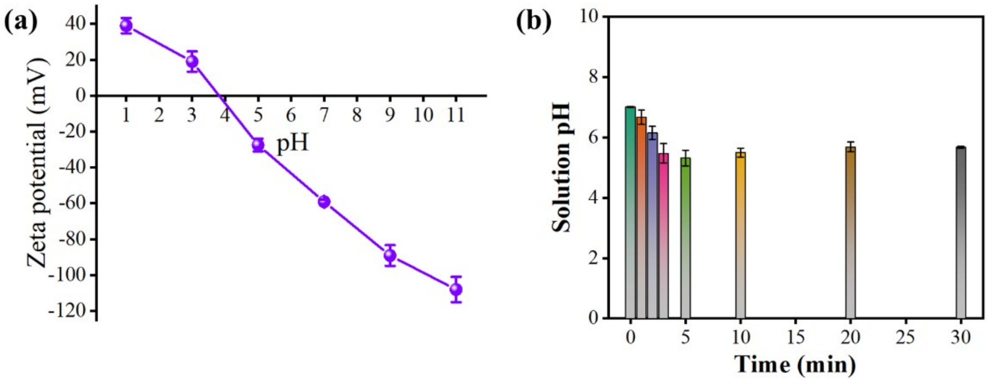

Fig. S8 Zeta potential analysis of Co_2TiO_4 (a), the change of solution pH during OFX degradation (b).

References

[1] L. Chen, S. Yang, X. Zuo, Y. Huang, T. Cai and D. Ding, *Chem. Eng. J.*, 2018, **354**, 856–865.

[2] L. Chen, T. Cai, W. Sun, X. Zuo and D. Ding, *J. Taiwan Inst. Chem. Eng.*, 2017, **80**, 720–727.

[3] M. Sayed, M. Gul, N. S. Shah, J. A. Khan, Z. U. H. Khan, F. Rehman, A. R. Khan, S. Rauf, H. Arandiyan and C. P. Yang, *J. Mol. Liq.*, 2019, **282**, 275–285.

[4] Y. Pi, P. Zhao, L. Ma, Y. Cao, H. Gao, S. Dong and J. Sun, *J. Alloys Compd.*, 2018, **747**, 721–728.

[5] Y. Pi, L. Ma, P. Zhao, Y. Cao, H. Gao, C. Wang, Q. Li, S. Dong and J. Sun, *J. Colloid Interface Sci.*, 2018, **526**, 18–27.

[6] G. Kresse and J. Furthmüller, *Phys. Rev. B*, 1996, **54**, 11169–11186.

[7] J. P. Perdew, K. Burke and M. Ernzerhof, *Phys. Rev. Lett.*, 1996, **77**, 3865–3868.

[8] G. Kresse and D. Joubert, *Phys. Rev. B*, 1999, **59**, 1758–1775.

[9] H. J. Monkhorst and J. D. Pack, *Phys. Rev. B*, 1976, **13**, 5188–5192.

[10] H. Wang, Q. Gao, H. Li, B. Han, K. Xia and C. Zhou, *Chem. Eng. J.*, 2019, **368**, 377–389.

[11] E. Hapeshi, I. Fotiou and D. Fatta-Kassinos, *Chem. Eng. J.*, 2013, **224**, 96–105.

[12] N. H. E Najjar, A. Touffet, M. Deborde, R. Journel and N. K. V. Leitner, *Chemosphere*, 2013, **93**, 604–611.

[13] Y. Gong, J. Li, Y. Zhang, M. Zhang, X. Tian and A. Wang, *J. Hazard. Mater.*, 2016, **304**, 320–328.

[14] N. De la Cruz, J. Giménez, S. Esplugas, D. Grandjean, L. Alencastro and C. Pulgarin, *Water Res.*, 2012, **46**, 1947–1957.

[15] K. S. Tay and N. Madehi, *Sci. Total Environ.*, 2015, **520**, 23–31.